Available online at www.sciencedirect.com
SCIENCE DIRECT®
Nuclear Instruments and Methods in Physics Research A 557 (2006) 585–593
NUCLEAR INSTRUMENTS & METHODS IN PHYSICS RESEARCH Section A
www.elsevier.com/locate/nima

Calibration of a neutron polarimeter in the 0.2–1.1 GeV region

A.Yu. Semenov[a,b,*,1], W.M. Zhang[a], R. Madey[a,c], A. Ahmidouch[a,2], B.D. Anderson[a], K. Assamagan[c,3], S. Avery[c], A.R. Baldwin[a], A.S. Crowell[d], T. Eden[c,4], D.M. Manley[a], P. Markowitz[e,f], G. Milleret[g,5], D. Prout[a,h,6], T. Reichelt[i], I.A. Semenova[a,b], P.E. Ulmer[j], E. Voutier[k], J.W. Watson[a], S.P. Wells[l,7]

[a]*Kent State University, Kent, OH 44242, USA*
[b]*Joint Institute for Nuclear Research, Dubna, Moscow region 141980, Russia*
[c]*Hampton University, Hampton, VA 23668, USA*
[d]*Duke University, Durham, NC 27708, USA*
[e]*Florida International University, FL 33199, USA*
[f]*Thomas Jefferson National Acceleration Facility, Newport News, VA 23606, USA*
[g]*Laboratoire National Saturne, 91191 Gif-sur-Yvette Cedex, France*
[h]*Indiana University Cyclotron Facility, Bloomington, IN 47408, USA*
[i]*Physikalische Institut Universität Bonn, D-53115 Bonn, Germany*
[j]*Old Dominion University, Norfolk, VA 23529, USA*
[k]*Laboratoire de Physique Subatomique et de Cosmologie, 38026 Grenoble, France*
[l]*Massachusetts Institute of Technology, Cambridge, MA 02139, USA*

Received 5 May 2005; received in revised form 27 October 2005; accepted 13 November 2005
Available online 12 December 2005

Abstract

We measured the analyzing power and the efficiency of a neutron polarimeter at the Saturne National Laboratory in France with central energies of the neutron beam of 261, 533, 752, 922, and 1057 MeV. This polarimeter was a prototype designed to measure G_E^n, the neutron electric form factor, at the Thomas Jefferson National Accelerator Facility.

PACS: 24.70.+s; 25.40.Dn; 29.30.Hs

Keywords: Neutron; Polarimeter; Scattering; Efficiency; Analyzing power

1. Introduction

Access to polarization observables is needed to reveal the structure of hadrons and nuclei and to understand the reaction mechanism in nuclear reactions. The polarization of medium-energy neutrons is usually measured with neutron polarimeters that utilize the analyzing power of spin-dependent elastic or quasielastic scatterings of the neutrons from unpolarized protons in nuclei. In a typical polarimeter, the front array consisted of plastic scintillator detectors and serves as an active polarization analyzer, while the scintillation rear arrays are configured to maximize the figure-of-merit (viz., to detect the maximum

*Corresponding author. Tel.: +1 631 344 5872.
E-mail address: semenov@jlab.org (A.Yu. Semenov).
[1]Present address: Department of Physics and Astronomy, Iowa State University, Ames, IA 50011, USA.
[2]Present address: North Carolina A & T University, Greensboro, NC 27411.
[3]Present address: CERN, EP Division, Geneva CH-1211, Switzerland.
[4]Present address: The National Center for Atmospheric Research (NCAR), Boulder, CO 80301.
[5]Present address: Laboratoire de Physique des Hautes Energies, Ecole Polytechnique, F91128 Palaiseau Cedex, France.
[6]Present address: DOE Remote Sensing Laboratory, Las Vegas, NV 89115.
[7]Present address: Louisiana Tech., Ruston, LA 71272.

0168-9002/$ - see front matter © 2005 Elsevier B.V. All rights reserved.
doi:10.1016/j.nima.2005.11.125

number of scattering events with the maximum scattering asymmetry) [1].

The use of a neutron polarimeter to measure G_E^n, the electric form factor of the neutron, in Bates experiment 85-05, was described earlier [2,3]. In a continuing effort to improve the quality of measurements and to extend the kinematic range for extracting G_E^n from the $^2H(\vec{e},e'\vec{n})^1H$ reaction, Madey [4] proposed a new configuration for a neutron polarimeter to be used at the Thomas Jefferson National Accelerator Facility (TJNAF) in experiment 93-038. The design of the polarimeter is based on the properties of n–p scattering for the analyzing reaction [1,5]. Advantages of the new configuration include a larger solid angle because of a larger frontal area; a higher efficiency because of an increased thickness of the front array; and the ability to operate in a high luminosity environment because the detectors in the rear array are shielded from the direct path of the neutron flux from the target.

We performed a calibration of a prototype neutron polarimeter for neutron energies between 261 and 1057 MeV with the neutron beam at the Saturne National Laboratory in France. An experiment [6] was performed earlier at the Indiana University Cyclotron Facility (IUCF) to calibrate a neutron polarimeter with a configuration similar to that of this neutron polarimeter; the IUCF calibration used the $^{14}C(\vec{p},\vec{n})^{14}N$ reaction for neutron energies below 200 MeV. In this paper, we describe the Saturne neutron beam and the experimental apparatus in Section 2, experimental procedures in Section 3, results in Section 4, efficiency simulation and comparison with measurements in Section 5, and conclusions in Section 6.

2. Beam and experimental apparatus

Fig. 1 shows the layout of the neutron polarimeter. It consists of 20 scintillation detectors: eight in the front array (1–8) and six in each of the two rear arrays (9–20) oriented parallel and lengthwise to the incident neutron flux. Each of the front eight (NE-102) plastic scintillators measured 25.4 cm × 101.6 cm × 10.16 cm. Each rear array consisted of two staggered layers of (NE-102) plastic scintillators; each layer was composed of three detectors positioned side by side and each detector measured 50.8 cm × 10.16 cm × 101.6 cm. Positioned immediately to the front and rear of the front array were thin (0.95-cm) plastic scintillation counters to veto (front) or tag (rear) charged particles. The neutron beam exited from a collimator with a circular hole 15 cm in diameter, and was incident on the center of the front array.

The polarimeter was symmetric with respect to the plane that includes the Y axis (vertical direction) and the Z axis (beam direction) in the Cartesian coordinate system. In these coordinates, the geometry of the detectors in the rear arrays is defined by locating the center of the 10th and 13th detectors at (56.7, 0.0, 235.0) (cm) and (71.9, 0.0, 269.5) (cm). At Saturne, we made measurements with two variations of the main configuration: one variation with the rear detector arrays raised by 25.4 cm, and the other raised by 46.5 cm. The purpose of these two variations was to simulate the case where neutrons interact away from the center of the front detectors.

The G_E^n experiments used a lead curtain ahead of the neutron polarimeter to degrade in energy high-energy photons produced at the target. To simulate the polarimeter operation with the lead curtain and to examine the possible depolarization of the neutron by the lead, we constructed a Fe–Pb–Fe wall consisting of 10 cm of lead sandwiched between two 3-cm steel plates and placed this wall 127 cm ahead of the front veto detector for some of the measurements.

3. Experimental procedures

The calibration was performed in May 1996 at the Saturne National Laboratory in France. Polarized neutrons at central energies of 261, 533, 752, 922, and 1057 MeV were produced by breakup of the polarized deuteron beam on a target that was either 4.0-cm thick Be, 0.159-cm thick Al, or 0.318-cm thick Al. The neutron beam was formed by an 8-m long collimator. The production target was 4.5 m upstream of the collimator or 12.5 m from the collimator exit. A sweeping magnet upstream of the collimator removed charged particles from the neutron beam. The collimator consisted of four cylindrical sleeves: (1) 9.5-cm diameter by 60-cm long; (2) 10.5-cm diameter by 90-cm long; (3) 11.5-cm diameter by 90-cm long; (4) 15-cm diameter by 5.6-m long. The neutron polarimeter was located about 1 m downstream from the exit of the collimator.

A beam-line polarimeter measured the polarization of the deuteron beam incident on the production target via the $d(\vec{d},p)t$ reaction at 386 keV [7]. A possible depolarization during acceleration from depolarizing resonances was studied carefully; no depolarizing effect was observed at a 2% level. To determine a deviation (arising from the D-state in the deuteron) of the polarization of a nucleon from the deuteron polarization, a Monte Carlo simulation was performed by Arvieux et al. [7] for the finite experimental geometry; the nucleon polarization was determined to be $(98.1 \pm 0.1)\%$ of the polarization of the deuteron beam incident on the production target. The mean polarization of neutrons P_n was found to be $(63.90 \pm 1.28)\%$.

3.1. Data structure

For each event, five parameters were recorded on magnetic tape: (1) The time-of-flight (ΔTOF) of a neutron scattered from a front detector to a rear detector; (2) the pulse-height in the front detector involved in the ΔTOF; (3) the pulse height in the rear detector involved in the ΔTOF; (4) the position of the interaction in the front detector; and (5) the position of the interaction in the rear detector. Tag

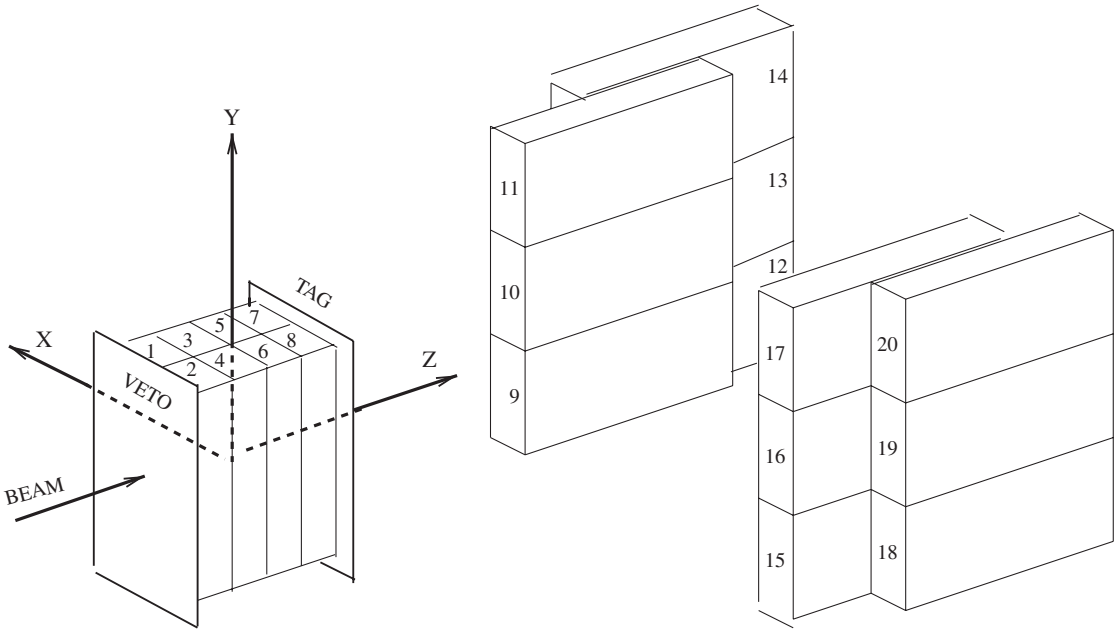

Fig. 1. Layout of the neutron polarimeter.

information regarding the spin status, the identification of charged particles, and the identification of any fired front and rear detectors was recorded also. The energy of a scattered neutron can be extracted from the first ΔTOF parameter.

3.2. Calibration of parameters

To extract physical information for an event, we needed calibration data for each of the five recorded parameters. The pulse-height calibration was done using the Compton spectrum from a ^{228}Th γ source placed at the external center of each scintillation detector. Details of the pulse-height calibration were described by Madey et al. [8]. The position was determined from the difference in the TDC signals from the PMT on each end of a detector. The position was calibrated with a linear conversion from the range of positions determined by the TDC signals to the physical length of the scintillation detector. To calibrate the ΔTOF time-of-flight, 96 spectra were extracted. Each of the 96 spectra represented the ΔTOF from one of the eight front detectors to one of the 12 rear detectors. A sharp peak was seen in each spectrum because the neutrons incident on the front detectors were nearly mono-energetic. This peak was used to determine the offset of a linear calibration for the ΔTOF spectrum. The slope (time per channel) of the linear calibration was calibrated to be 93.7 ps/channel with a precision time calibrator (Tennelec Model TC 850). Out of the 96 offsets (off_{ij}), only 20 were independent because there were 20 independent parameters with each representing a time delay in cables and electronics associated with a detector. A fit was used to reduce the number of calibration constants from 96 to 20.

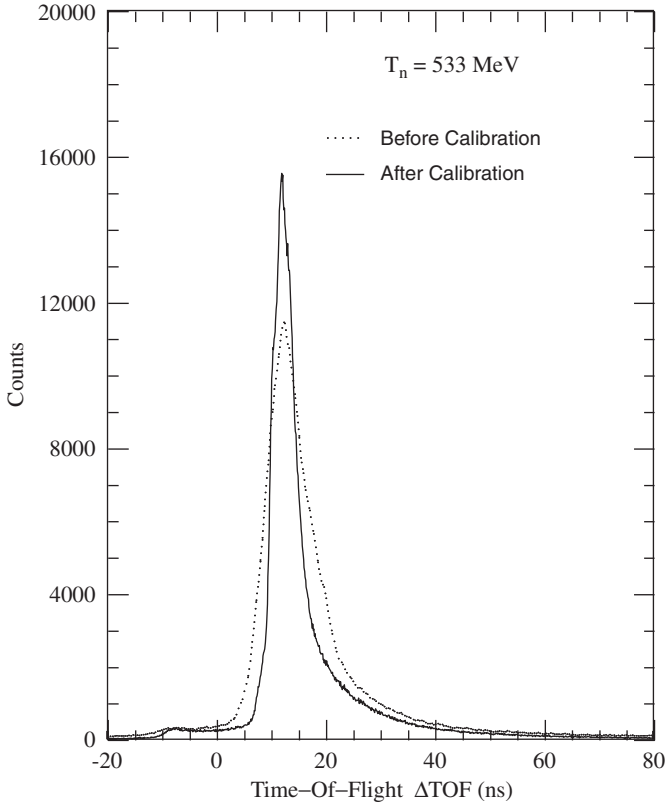

Fig. 2. Neutron time-of-flight from a front detector to a rear detector for incident neutrons at 533 MeV. Dotted and solid lines represent the spectrum before and after calibration, respectively.

Eight of the 20 constants (f_i) were associated with the eight front detectors and 12 of them (r_j) were associated with the 12 rear detectors. A set of 96 new correlated offsets (off'_{ij})

was calculated from f_i and r_j, where each off'_{ij} was just the sum of f_i and r_j. Fig. 2 shows typical ΔTOF time-of-flight spectra before and after the calibration; these spectra represent the sum over time-of-flights contributed by 96 pairs of one front detector and one rear detector.

3.3. Trigger and its efficiency

A coincidence between a detector in the front array and a detector in the rear array was used to generate the trigger. Any subsequent triggers occurring before the current event conversion and computer readout were not recorded, resulting in dead-time. One of the two inputs of the coincidence module was a narrow pulse (10 ns) that was the OR signal of all front detectors above the hardware threshold; the other was the window pulse (200 ns) of the OR signal of all rear detectors above the hardware threshold. The narrow pulses were counted by a scaler, which registered a single count if pulses from separate detectors were within 10 ns of each other. The tag words recorded events from front and rear detectors that occurred within a 6 μs acquisition interval. The scaler counted the number of triggers generated by the data acquisition (DAQ) system. Only a fraction of the triggered events was recorded because of the DAQ dead-time. In this experiment, two clocks were setup to measure the live-time fraction of the DAQ system. One clock recorded the live-time t_l of the ADC modules, and the other recorded the elapsed time t_e. The live-time fraction τ was calculated as the ratio of the live-time to the elapsed time during the time that the beam pulse was on: $\tau = t_l/t_e$. The beam spill duration was typically 900 ms for neutron energies of 261, 533, and 752 MeV, and 500 ms for neutron energies of 922, and 1057 MeV; the beam was continuous inside the spill. The live-time fractions averaged over the runs at each of these energies are plotted in Fig. 3a. The large uncertainties in the live-time fraction τ reflect the fluctuations in the effective beam duty factor.

The trigger efficiency $\varepsilon_{\mathrm{trig}}$ after the correction for the live-time fraction τ was estimated with

$$\varepsilon_{\mathrm{trig}} = \frac{N_{\mathrm{tape}}}{\tau I} \tag{1}$$

where N_{tape} is the number of events recorded on tape, and I is the number of incoming neutrons. The number of incident neutrons I was estimated with

$$I = \frac{(1-R)(N_1+N_2)-V}{\varepsilon_1} \tag{2}$$

where N_1 and N_2 are the number of counts in the first (left) and the second (right) detector, respectively, in the first layer of the front array, V is the number of counts in the veto detector, R is the ratio of the number of counts for the case where both the first and the second detector are triggered to the sum of N_1 and N_2, and ε_1 is the detection efficiency of a front scintillator. The ratio R was used to correct for double counting. The ratio R was estimated

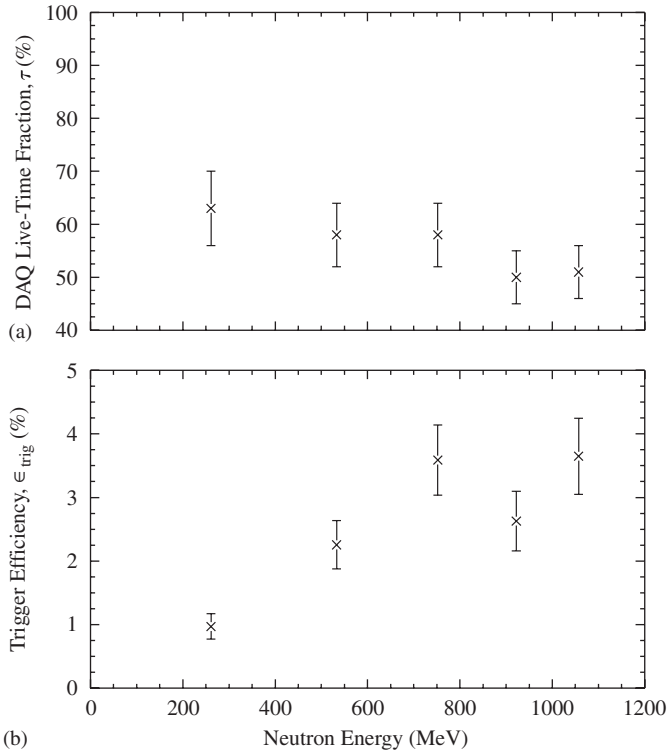

Fig. 3. DAQ live-time fraction (panel a) and trigger efficiency (panel b) after correction for the DAQ live-time as a function of the neutron beam energy.

with the recorded tag information assuming that the multiplicity distribution of events was not changed after the trigger; although the ratio R in Eq. (2) should be the one before the trigger, we extracted R from the data on tape. The ratio R is about 10%. A difference of 10–20% in R before and after the trigger would make only a 1–2% change in the value of I in Eq. (2). The neutron detection efficiency ε_1 of a front detector was estimated with the Monte Carlo code of Cecil et al. [9]. Fig. 3b shows $\varepsilon_{\mathrm{trig}}$, the trigger efficiency corrected for the live-time fraction, as a function of the energy of the incident neutron.

The trigger efficiencies obtained in this way would be underestimated if the flux of neutral particles incident on the polarimeter contained a significant fraction of photons. The thickness in radiation lengths of the Fe–Pb–Fe wall was sufficient to attenuate photons produced in the incident neutron beam by the deuteron stripping process. The fact that the difference between the efficiencies observed with and without the Fe–Pb–Fe wall is smaller than the uncertainties implies that the fraction of photons in the neutron beam incident on the Fe–Pb–Fe wall is small or comparable to the photon fraction in the neutron beam emerging from the Fe–Pb–Fe wall.

A Monte Carlo simulation estimated the photon flux generated in the Fe–Pb–Fe wall. The simulation program, based on GEANT 3.21 [10], uses the GCALOR [11] program package to simulate hadronic interactions down to 1 MeV for nucleons and charged pions and into the

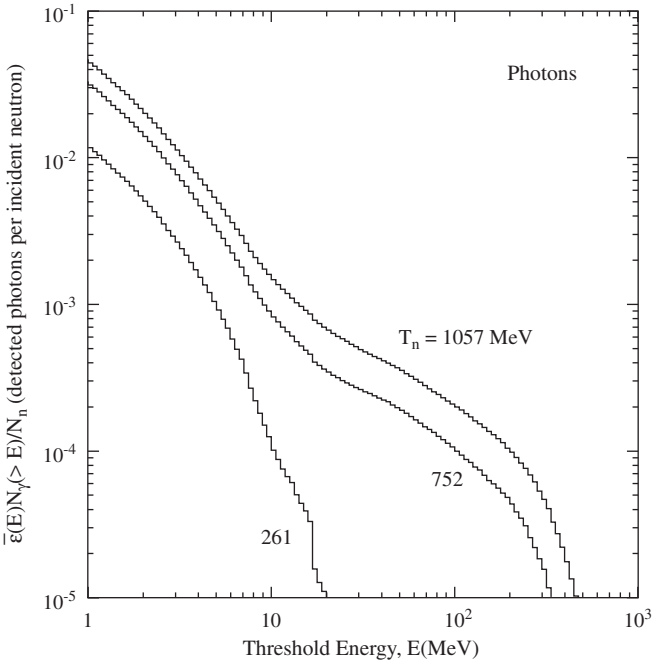

Fig. 4. The integral detection rates of photons in a 10.16-cm thick plastic scintillator for incident neutron energies of 261, 752, and 1057 MeV.

thermal region for neutrons, and DINREG [12,13]—Deep Inelastic Nuclear Reaction Exclusive Generator with a model for hadronic interactions of electrons and photons.

Neutrons with kinetic energies of 261, 533, 752, 922, and 1057 MeV were assumed to originate from a cylindrical volume, 2-cm in diameter and 4-cm thick, placed at the position of the Be or Al target bombarded by polarized deuterons to produce the neutron beam. Per neutron emanating from the target volume, the integral detection rate of photons above 4 MeVee in a 10.16-cm plastic scintillator was a small fraction of the integral detection rate of neutrons above 8.4 MeV (= 4 MeVee, where MeVee denotes MeV of equivalent electron energy). The Monte Carlo results for the photon-to-neutron ratio (in percent) were 6.2, 10.0, 13.4, 15.8, and 17.5 for incident neutron energies, respectively, of 261, 533, 752, 922, and 1057 MeV. The integral detection rates of photons in a 10.16-cm plastic scintillator are shown in Fig. 4 for incident neutron energies of 261, 752, and 1057 MeV. A lesser fraction of these photons would Compton scatter from the front array to the rear array of the polarimeter to contribute to N_{tape}, the number of events recorded on tape. We conclude that the trigger efficiencies quoted here might be underestimated slightly.

3.4. Event selection and its efficiency

While the trigger efficiency is hardware related, the selection efficiency depends on software cuts. Off-line, single-hit events were selected according to four criteria: Events were rejected if (1) the scattered particle was identified as charged by the charged particle tag detector; (2) the event was triggered by more than one front detector or by more than one rear detector; (3) the event fell below software pulse-height thresholds (4 MeVee for the front detectors and 10 MeVee for the rear detectors); or (4) if the scattered neutron was from the inelastic C(n, np) reaction. To determine if a scattered neutron came from the inelastic reaction, we calculated a velocity ratio $R_V = V_{sc}/V_{np}$, where V_{sc} is the speed of the scattered neutron calculated from the measured flight time and the geometric path length, and V_{np} is the speed of a neutron associated with n–p scattering. The speed V_{np} was calculated with

$$V_{np} = \frac{(T_{np}^2 + 2T_{np}M)^{1/2}}{(T_{np} + M)} \tag{3}$$

where M is the neutron mass and T_{np} is the kinetic energy of the scattered neutron. The kinetic energy T_{np} was calculated as

$$T_{np} = \frac{2T_n \cos^2\theta}{[(\gamma+1) - (\gamma-1)\cos^2\theta]} \tag{4}$$

where T_n is the kinetic energy of the incident neutron, θ is the angle of the scattered neutron, and γ is the ratio of the total energy of the incident neutron to its mass. A typical spectrum of the velocity ratio R_V is shown in Fig. 5. Events from neutrons scattered inelastically usually had a low

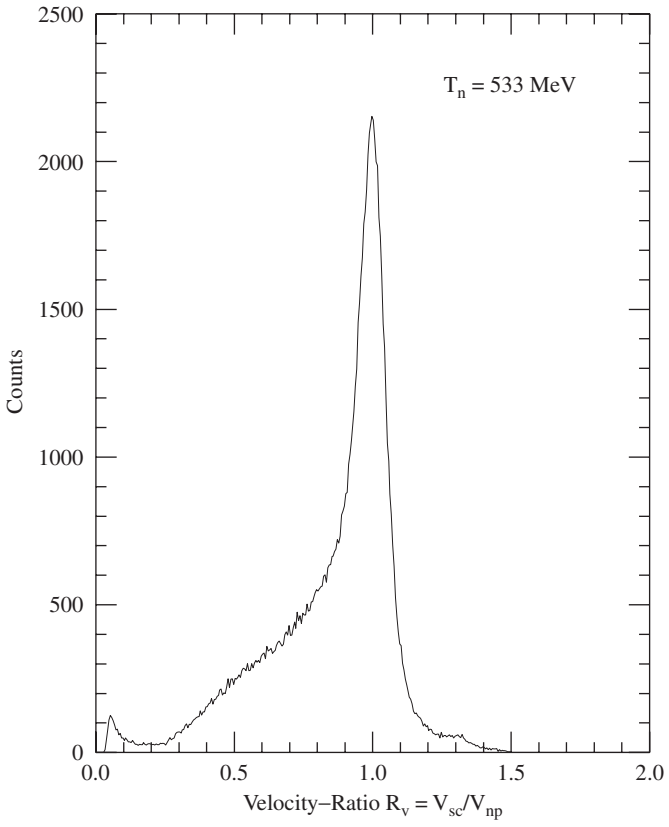

Fig. 5. Neutron velocity-ratio R_V spectrum for incident neutrons at 533 MeV.

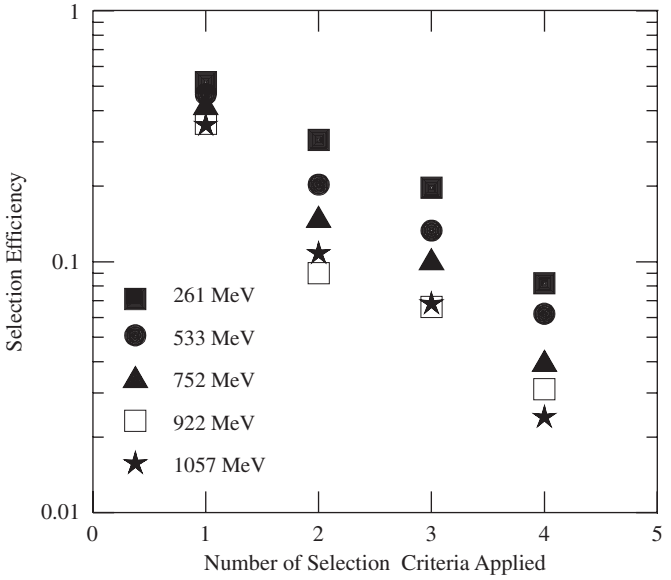

Fig. 6. Selection efficiencies as a function of number of selection criteria applied in consecutive order (see text) for neutrons at six incident energies. The fourth selection criterion here corresponds to a velocity-ratio $R_V > 0.95$.

value of R_V. For each neutron energy, Fig. 6 shows the fraction of events that survive after successive application of the four selection criteria; for example, after applying all four selection criteria, 4% of the events survive at 752 MeV. The fourth selection efficiency shown in Fig. 6 corresponds to a velocity-ratio value $R_V > 0.95$ (i.e., we selected events with kinematics most close to that expected for neutron–proton elastic scattering). The detection efficiency ε of the neutron polarimeter is the product of the trigger efficiency after correction for the live-time fraction and the selection efficiency:

$$\varepsilon = \varepsilon_{\text{trig}}\varepsilon_{\text{select}}. \tag{5}$$

4. Results and summary

After imposing four criteria, we obtained four velocity-ratio spectra that depended on the polarization state (U = spin Up or D = spin Down) of the incident neutrons and the scattering state (L = Left or R = Right) of scattered neutrons. From these spectra, we obtained for each spin state N_L^U, N_R^U, N_L^D, N_R^D, the number of neutrons scattered to the left and to the right. We employed the cross-ratio technique [14] to calculate the scattering asymmetry ξ:

$$\xi = \frac{(r-1)}{(r+1)}. \tag{6}$$

The cross ratio r is the ratio of the two geometric means $(N_L^U N_R^D)^{1/2}$ and $(N_R^U N_L^D)^{1/2}$:

$$r = \left[\frac{(N_L^U N_R^D)}{(N_R^U N_L^D)}\right]^{1/2}. \tag{7}$$

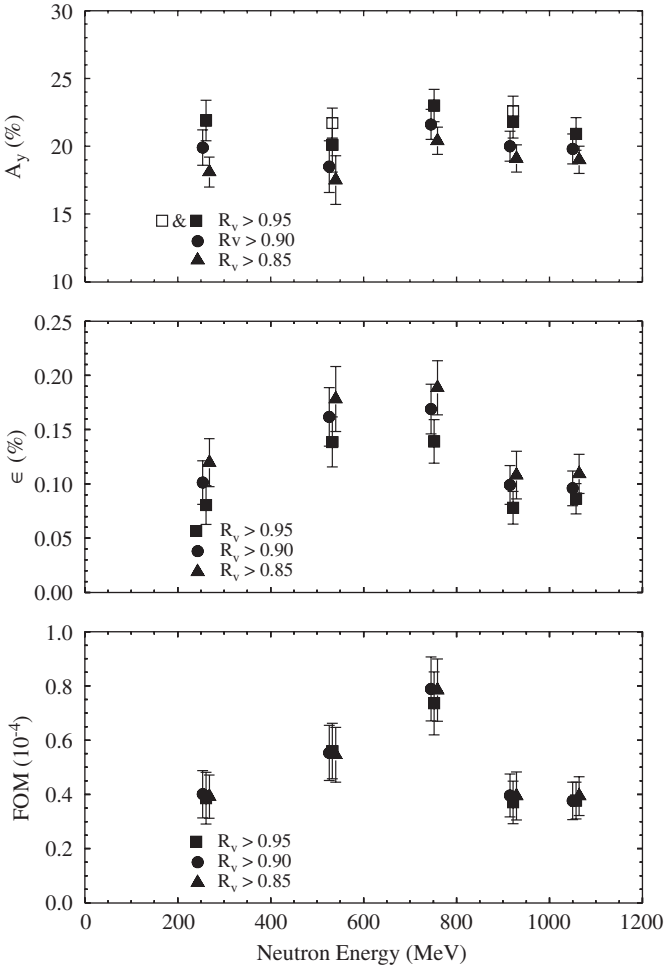

Fig. 7. Experimental results for the analyzing power A_y, the polarimeter efficiency ε, and the polarimeter figure-of-merit FOM for events with a single hit in the front and a single hit in the rear array. With an increasing R_V ratio, A_y increases and ε decreases; but the FOM is insensitive to R_V. Closed and open symbols represent results with and without a lead-steel wall, respectively.

Then, the analyzing power is given by

$$A_y = \frac{\xi}{P_n} \tag{8}$$

where P_n is the neutron polarization.

The top panel in Fig. 7 shows the analyzing power A_y as a function of the incident neutron energy for three different values of the R_V ratio. Closed symbols represent results from measurements with the Fe–Pb–Fe wall. The A_y values are an average over all measurements with the rear detectors in different Y positions whenever such measurements were performed. (The results from the measurements with the rear detectors lifted are not significantly different from those without lifting because the mean scattering angle of neutrons is changed only slightly with the rear detectors lifted). The uncertainties in A_y are dominated by the systematics that arose from the uncertainties in the calibration for the recorded parameters described in

Section 3.2. The parameters that introduce the greatest uncertainty are uncertainties in the estimation and subtraction of background.

The analyzing power A_y without a Fe–Pb–Fe wall was measured at incident neutron energies of 533 and 922 MeV. These measurements are shown as the two open squares in Fig. 7; they indicate a possible small depolarization in the Fe–Pb–Fe wall. This result is consistent with our previous report [2] that there may be a neutron depolarization of about 5% in the Fe–Pb–Fe wall.

The middle panel of Fig. 7 shows the polarimeter efficiency ε (see Eq. (5)) for three values of the R_V ratio after correction for the DAQ live-time fraction. The large uncertainties in the polarimeter efficiencies ε are mostly inherited from the uncertainties in the trigger efficiencies. The bottom panel of Fig. 7 shows the figure-of-merit $\mathrm{FOM} = \varepsilon A_y^2$ as a function of the incident neutron energy for three values of R_V. Note that the FOM is insensitive to R_V, whereas A_y increases with R_V while the efficiency decreases as R_V increases.

5. Efficiency and analyzing power from JLab E93-038

In 2000/2001, the electric form factor of neutron was measured via recoil polarimetry in Experiment 93-038 at Thomas Jefferson National Accelerator Facility [15]. A beam of longitudinally polarized electrons (with a typical polarization of 80%) scattered quasielastically from a neutron in a 15-cm liquid deuterium target. A scattered electron was detected in the High Momentum Spectrometer in coincidence with the recoil neutron. For a fixed neutron scattering angle of 46.0°, beam energies of 0.884, 2.33, and 3.40 GeV were associated with average energies of the recoil neutron of 239, 606, and 786 MeV, respectively. The neutron polarimeter used in E93-038 contained a few improvements, which were applied to increase the polarimeter efficiency and to achieve luminosities of $\sim 3 \times 10^{38}\,\mathrm{cm^{-2}\,s^{-1}}$. The polarimeter consisted of a total of 44 plastic scintillation detectors. The front array was segmented into 20 detectors [100 cm × 10 cm × 10 cm] arranged into four layers. Top and bottom rear arrays were shielded from the direct path of particles from the target. Each rear array consisted of 6 "20-in" detectors [101.6 cm × 50.8 cm × 10.16 cm] and 6 "10-in" detectors [101.6 cm × 25.4 cm × 10.16 cm]. A double layer of "veto/tagger" detectors (each 0.64-cm thick) directly ahead of and behind the front array identified incoming and scattered charged particles. A 10-cm lead curtain attenuated the flux of electromagnetic radiation and charged particles incident on the polarimeter. The flight path from the center of the target to the center of the front array was 7.0 m, and the mean flight path from the front array to the rear array was 2.5 m.

To figure out the mean value of the recoil neutron polarization, we averaged Arenhövel's theoretical $^2\mathrm{H}(\vec{e}, e'\vec{n})^1\mathrm{H}$ calculations [16] over the experimental acceptance. These calculations include leading-order relativistic contributions to a non-relativistic model of the deuteron as an n–p system, employ the Bonn R-space NN potential [17] for the inclusion of FSI, and include MEC and IC. Other realistic potentials (e.g., the Argonne V18 [18]) give essentially the same results. Recoil polarizations were calculated for the values of the ratio of the neutron electric and magnetic form factors, $g \equiv G_E^n/G_M^n$, measured in E93-038.

The polarimeter used in E93-038 contained three layers of scintillation detectors in each of the rear arrays while the polarimeter prototype tested at the Saturne National Laboratory in 1996 contained two layers of detectors in each of the rear arrays. To be consistent with the prototype calibration conditions, we selected the events that were recorded in only the two inner layers of the rear detectors. To equilibrate the fine segmentation of the E93-038 polarimeter, we united (viz., considered as coming from the same detector) the signals from the top two and the bottom three detectors in each layer of the front array in the data analysis; similarly, we united the signals from the two "10-in" detectors in each layer of the rear array. Finally, the event selection criteria for single-hit events were applied; we used a velocity-ratio selection criterion $R_V > 0.95$. The efficiency was estimated as

$$\varepsilon \approx \frac{N_n}{N_0} \tag{9}$$

where N_n is the number events registered in the E93-038 polarimeter that met the selection criteria; and N_0, the flux of the neutrons from the quasielastic $d(\vec{e}, e'\vec{n})$ reaction incident on the polarimeter front array, was obtained from a simulation performed with the MCEEP program [19]. The polarimeter efficiency values (corrected for a neutron transmission of 0.57 through the 10-cm lead curtain) are shown in Fig. 8(top panel) as empty squares. Also shown in the top panel of Fig. 8 are the results of the neutron efficiency of the prototype polarimeter simulated with the FLUKA 2002.1b code [20]. The efficiency values extracted from both JLab E93-038 measurements and the simulation with FLUKA 2002.1b agree with the results of the polarimeter prototype test at the Saturne National Laboratory.

The bottom panel of Fig. 8 compares the values of the polarimeter analyzing power extracted from JLab E93-038 with those from the prototype polarimeter calibration at the Saturne National Laboratory. The analyzing power value from JLab E93-038 at the neutron kinetic energy of 239 MeV is slightly higher than one from the prototype test. The possible explanation of this difference is that the better coordinate and time resolutions of the polarimeter used in JLab E93-038 provided a more reliable selection of n–p scattering events in TJNAF experiment.

The JLab E93-038 polarimeter has a high FOM and is capable of operating at high luminosities. To evaluate the performance of different polarimeters, it is necessary to incorporate the frontal area S into the figure-of-merit:

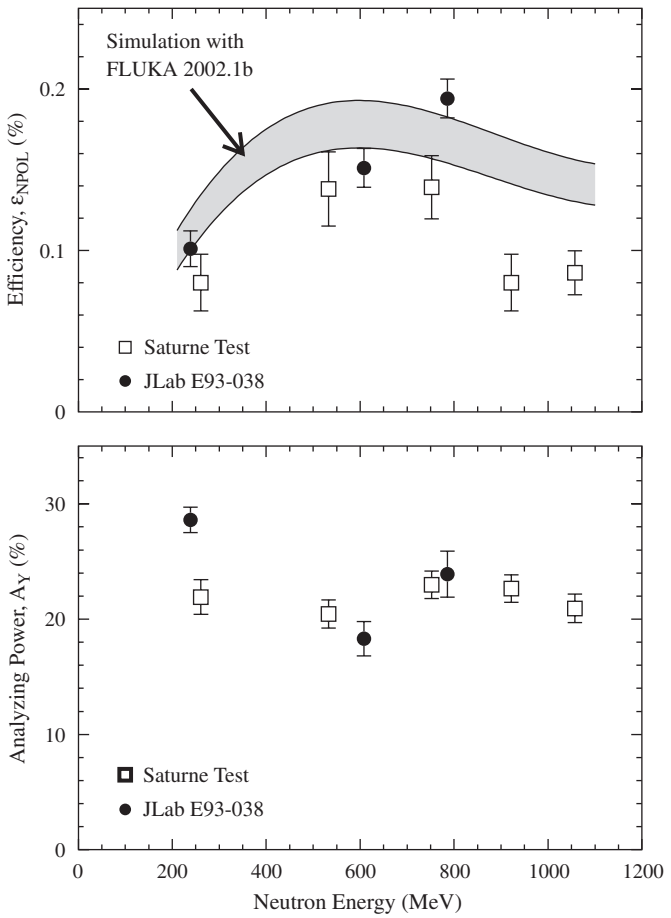

Fig. 8. Comparison of the prototype polarimeter parameters (viz., neutron polarimeter efficiency and analyzing power) measured at the Saturne National Laboratory (open boxes) with the results from E93-038 (closed circles). The gray band in the top panel shows the uncertainty in the polarimeter efficiency simulated with the FLUKA 2002.1b code. The results correspond to a velocity-ratio selection criterion $R_V > 0.95$.

FOM $= \varepsilon A_y^2 S$. Values of this FOM are given in Ref. [1] for several polarimeters. For the polarimeter used in JLab E93-038, $S = 5000\,\text{cm}^2$ (with a front array height of 50 cm), $\varepsilon \approx 0.01$ (with a front array thickness of 40 cm), and $A_y \approx 0.16$ (for 750 MeV neutrons); thus, FOM $\approx 1.3\,\text{cm}^2$, which is higher than that for any polarimeter in Ref. [1]. At the same neutron energy, the polarimeter designed for the new JLab Experiment 04-110 will have a still higher FOM primarily because $S = 12,000\,\text{cm}^2$ (with a front array height of 120 cm), and the front array thickness is being increased to 50 cm.

6. Conclusions

We calibrated a prototype of a neutron polarimeter for Experiment 93-038 at TJNAF, and we demonstrated a technique that is suitable for measuring the analyzing power and the efficiency of the neutron polarimeter. The analyzing power of the polarimeter is approximately constant for neutron energies from 0.2 to 1.1 GeV. The prototype polarimeter efficiency and analyzing power are in reasonable agreement with values extracted from JLab E93-038. Simulation of the neutron efficiency with FLUKA 2002.1b code support both the results of the prototype polarimeter test at Saturne National Laboratory and the polarimeter efficiency extracted from JLab E93-038 measurements.

Acknowledgements

This research was supported in part by the National Science Foundation under Grant Nos. PHY-94-09265, PHY-96-00665, PHY-97-22533, PHY-01-39913, HRD-96-33750, the Department of Energy Contract DE-AC05-84ER40150, the Thomas Jefferson National Accelerator Facility, and Deutsche Forschungsgesellschaft. We acknowledge the excellent support of the staff of the Saturne National Laboratory.

References

[1] R. Madey, A.R. Baldwin, P.J. Pella, J. Schambach, R.M. Sellers, IEEE Trans. Nucl. Sci. NS-36 (1989) 231.
[2] T. Eden, et al., Nucl. Instr. and Meth. A 338 (1994) 432.
[3] T. Eden, et al., Phys. Rev. C 50 (1994) R1749.
[4] R. Madey, A. Lai, T. Eden, Proceedings of the AIP Conference, Vol. 339, 1995, pp. 47–54.
[5] J. Watson, M.R. Plumley, P.J. Pella, B.D. Anderson, A.R. Baldwin, R. Madey, Nucl. Instr. and Meth. A 272 (1988) 750.
[6] I. Niculescu, et al., IEEE Trans. Nucl. Sci. NS-45 (1998) 68 The paper is available electronically via IEEE web: ⟨http://www.ieeexplore.ieee.org/iel5/23/14376/00659556.pdf⟩.
[7] J. Arvieux, S.D. Baker, A. Boudard, J. Cameron, T. Hasegawa, D. Hutcheon, C. Kerboul, G. Gaillard, V.-S. Nguyen, Nucl. Instr. and Meth. A 273 (1988) 48.
[8] R. Madey, et al., Nucl. Instr. and Meth. A 214 (1983) 401.
[9] R. Cecil, B.D. Anderson, R. Madey, Nucl. Instr. and Meth. 161 (1979) 439.
[10] R. Brun, et al., CERN Program Library Long Writeup W5013, September, 1993.
[11] C. Zeitnitz, T.A. Gabriel, Nucl. Instr. and Meth. A 349 (1994) 106.
[12] P.V. Degtyarenko, M.V. Kossov, Preprint ITEF 11-92, Moscow, 1992.
[13] P.V. Degtyarenko, M.V. Kossov, H.-P. Wellisch, Eur. Phys. J. A 8 (2000) 217;
P.V. Degtyarenko, M.V. Kossov, H.-P. Wellisch, Eur. Phys. J. A 9 (2000) 411;
P.V. Degtyarenko, M.V. Kossov, H.-P. Wellisch, Eur. Phys. J. A 9 (2000) 421.
[14] G.G. Ohlsen, P.W. Keaton Jr., Nucl. Instr. and Meth. 109 (1973) 41.
[15] R. Madey, et al., Phys. Rev. Lett. 91 (2003) 122002.
[16] H. Arenhövel, W. Leidemann, E.L. Tomusiak, Phys. Rev. C 52 (1995) 1232;
H. Arenhövel, W. Leidemann, E.L. Tomusiak, Phys. Rev. C 46 (1992) 455;
H. Arenhövel, W. Leidemann, E.L. Tomusiak, Z. Phys. A 331 (1988) 123;
H. Arenhövel, W. Leidemann, E.L. Tomusiak, Z. Phys. A 334 (1989) 363(E);
H. Arenhövel, Private communication, 2002, 2003.
[17] R. Machleidt, K. Holinde, Ch. Elster, Phys. Rep. 149 (1987) 1.

[18] R.B. Wiringa, V.G.J. Stoks, R. Schiavilla, Phys. Rev. C 51 (1995) 38.
[19] P.E. Ulmer, MCEEP—Monte Carlo for Electro-Nuclear Coincidence Experiments, CEBAF-TN-91-101, 1991.
[20] A. Fasso, A. Ferrari, P.R. Sala, Electron–photon transport in FLUKA: status, in: A. Kling, F. Barao, M. Nakagawa, L. Tavora, P. Vaz (Eds.), Proceedings of the Monte Carlo 2000 Conference, Lisbon, October 23–26, 2000, Springer, Berlin, 2001, pp. 159–164;
A. Fasso, A. Ferrari, J. Ranft, P.R. Sala, FLUKA: status and perspective for hadronic applications, in: A. Kling, F. Barao, M. Nakagawa, L. Tavora, P. Vaz (Eds.), Proceedings of the Monte Carlo 2000 Conference, Lisbon, October 23–26, 2000, Springer, Berlin, 2001, pp. 955–960.